Molecular Pharmacology Fast Forward. Published on February 6, 2017 as DOI: 10.1124/mol.116.107755
This article has not been copyedited and formatted. The final version may differ from this version.

Title Page

Structural and Preclinical Studies of Computationally-Designed Non-nucleoside Reverse Transcriptase Inhibitors for Treating HIV infection

Shalley N. Kudalkar, Jagadish Beloor, Albert H. Chan, Won-Gil Lee, William L. Jorgensen, Priti Kumar, and Karen S. Anderson

Department of Pharmacology, Yale University School of Medicine, New Haven, Connecticut, United States (SNK, AHC, KSA); Department of Chemistry, Yale University, New Haven, Connecticut, United States (WL, WJ); School of Medicine, Infectious Diseases/Internal Medicine, Yale University, New Haven, Connecticut (JB, PK)

Molecular Pharmacology Fast Forward. Published on February 6, 2017 as DOI: 10.1124/mol.116.107755
This article has not been copyedited and formatted. The final version may differ from this version.

Running Title Page

Running Title: *Computationally designed potent NNRTIs with enhanced in vivo pharmacokinetics*

Corresponding Authors: Karen S. Anderson, Department of Pharmacology Sterling Hall of Medicine, B-Wing, 333 Cedar Street, New Haven, CT 06510, Phone: 203.785.4526, Fax: 203.785.7670, E-mail: karen.anderson@yale.edu

Priti Kumar, School of Medicine, Infectious Diseases/Internal Medicine, P.O. Box 208022 25 York Street, New Haven, CT 06510, Phone: 203.737.3580, Email: priti.kumar@yale.edu

Number of text pages: 31

Number of tables: 2

Number of figures: 8

Number of references: 46

Number of words in:

Abstract: 285

Introduction: 752

Discussion: 1364

Abbreviations

HIV, Human immunodeficiency virus, HIV-RT, HIV reverse transcriptase, NNRTI, Non-nucleoside reverse transcriptase inhibitor, EC_{50}, Half maximal effective concentration of a compound, IC_{50}, Half maximal inhibitory concentration of a compound, HPLC, High performance liquid chromatography, PK, Pharmacokinetics, C_{max}, The maximum concentration of a drug observed in serum after its administration, T_{max}, The time taken to reach C_{max}, AUC, A plot of concentration of drug in blood plasma against time, CL, Clearance

Molecular Pharmacology Fast Forward. Published on February 6, 2017 as DOI: 10.1124/mol.116.107755
This article has not been copyedited and formatted. The final version may differ from this version.

Abstract

The clinical benefits of human immunodeficiency virus type 1 (HIV-1) non-nucleoside reverse transcriptase (RT) inhibitors (NNRTIs) are hindered by their unsatisfactory pharmacokinetic (PK) properties along with the rapid development of drug-resistant variants. However, the clinical efficacy of these inhibitors can be improved by developing compounds with enhanced pharmacological profiles and heightened antiviral activity. We used computational and structure-guided design to develop two next-generation NNRTI drug candidates, compounds I and II, which are members of a class of catechol diethers. We evaluated the preclinical potential of these compounds in BALB/c mice because of their high solubility (510 µg/mL for compound I and 82.9 µg/mL for compound II), low cytotoxicity and enhanced antiviral activity against wild type (WT) HIV-1 RT and resistant variants. Additionally, crystal structures of compounds I and II with WT RT suggested an optimal binding to the NNRTI binding pocket favoring the high anti-viral potency. A single intraperitoneal dose of compounds I and II exhibited a prolonged serum residence time of 48 h and concentration maximum (C_{max}) of 4000-15 000 fold higher than their therapeutic / effective concentrations. These C_{maxs} were 4-15 fold lower than their cytotoxic concentrations observed in MT-2 cells. Compound II showed enhanced $AUC_{(0\text{-last})}$ and decreased plasma clearance over compound I and efavirenz, the standard of care NNRTI. Hence, the overall PK profile of compound II was excellent compared to that of compound I and efavirenz. Furthermore, both compounds were very well tolerated in BALB/c mice without any detectable acute toxicity. Taken together, these data suggest that compounds I and II possess improved anti-HIV-1 potency, remarkable *in vivo* safety and prolonged *in vivo* circulation time suggesting strong potential for further development as new NNRTIs for the potential treatment of HIV infection.

Molecular Pharmacology Fast Forward. Published on February 6, 2017 as DOI: 10.1124/mol.116.107755
This article has not been copyedited and formatted. The final version may differ from this version.

Introduction

Globally, it is estimated that 36.7 million people are infected with the human immunodeficiency virus (HIV); progression of the infection to acquired immunodeficiency syndrome (AIDS) causes over 1.1 million complications-related deaths per year. The current standard of care for therapeutically treating HIV infection is a minimum of three different antiretroviral drugs as a part of highly active antiretroviral therapy (HAART). Non-nucleoside reverse transcriptase inhibitors (NNRTIs) are major components of HAART. These drugs significantly inhibit the catalytic function of HIV-reverse transcriptase (RT) by binding in an allosteric binding pocket 10-Å away from the RT polymerase active site and affect the chemical step of DNA synthesis (de Bethune, 2010; Fulco and McNicholl, 2009; Spence et al., 1996; Spence et al., 1995). Two of the five FDA-approved NNRTIs, efavirenz and rilpivirine (Figure 1A and B), are key components of the FDA-approved fixed dose therapies Atripla™, Complera™, and Odefsey™(Fellner, 2016; Permpalung et al., 2012).

In addition to the problem of promoting drug-resistance, the clinical benefits of both of these drugs are hindered by their unsatisfactory pharmacokinetic (PK) properties. Their high cytotoxicity and poor aqueous solubility leads to low bioavailability and difficulties in formulation requiring high dosage (Huang et al., 2015). Additionally, rapid blood clearance and insufficient drug concentration *in vivo* necessitates higher dosing which results in high pill burden, lowered patient compliance and development of cross-resistance between drug classes (Delaugerre et al., 2001). Furthermore, efavirenz's low genetic barrier to resistance requires high-level adherence to therapy for efficacy (Delaugerre et al., 2001; Riddler et al., 2008). HIV-infected patients receiving efavirenz also suffer from side effects such as depression, insomnia, skin rash, lipodystrophy, and lipoatrophy (de Waal et al., 2013; Riddler et al., 2008). On the other hand, rilpivirine prescription requires a heightened vigilance in clinical practice due to its unfavorable interaction with acid suppressant medication (Janssen et al., 2005; Rathbun and Liedtke, 2011). Furthermore, as a substrate of CYP34A, rilpivirine cannot be co-administered

Molecular Pharmacology Fast Forward. Published on February 6, 2017 as DOI: 10.1124/mol.116.107755
This article has not been copyedited and formatted. The final version may differ from this version.

with drugs that are CYP3A4 inducers (Janssen et al., 2005; Riddler et al., 2008). Moreover, preclinical studies with rilpivirine (Edurant^{TM}) reveal inhibition of hERG ion channel and clinical trials in Canada demonstrating prolongation of QT intervals in patients at higher dosing, prompt concerns of cardiotoxicity (http://www.hc-sc.gc.ca/dhp-mps/prodpharma/sbd-smd/drug-med/sbd_smd_2011_edurant_137484-eng.php;Summary Basis of Decision, 137484, Health Canada). Therefore, development of alternative NNRTIs may prove beneficial for HIV-infected individuals, especially those who have experienced virologic failure.

To address the poor pharmacokinetic properties and issues of toxicity with currently approved NNRTIs, using computational and structure guided design; we successfully developed two next-generation NNRTI drug candidates, referred to as compound I and compound II (Figure 1C and D). These compounds belong to a potent class of inhibitors known as catechol diethers, which possess better aqueous solubility, low cytotoxicity, and increased potency towards wild type (WT) and resistant strains of HIV-1 (Lee et al., 2014; Lee et al., 2013). Compound I demonstrates picomolar activity (310 pM) against WT RT and low nano-molar activity toward clinically challenging variants (Lee et al., 2014), likely resulting from its molecular flexibility at the NNRTI binding pocket (NNBP) (Frey et al., 2015). Compound II possesses low nano-molar potency (1.9 nM) for WT RT and has very low cytotoxicity (>100 µM) (Lee et al., 2014). These encouraging findings prompted us to further investigate compounds I and II as potential anti-HIV drug candidates. We explored the pharmacokinetic profiles and single dose safety and tolerance of both compounds in BALB/c mice. In addition, the compounds were evaluated for potential off-target effects on a panel of 34 molecular targets including ion channel, receptors, and cytochrome P450 enzymes. Our pharmacological goal was to achieve serum concentrations that are expected to provide complete inhibition of RT based on a cell culture model of HIV-inhibition. Indeed, pharmacokinetics analyses showed that the C_{max} for both compounds in BALB/c mice were several-fold higher than those required for inhibition of WT and resistant strains of HIV virus in cellular assays. Additionally, both compounds

Molecular Pharmacology Fast Forward. Published on February 6, 2017 as DOI: 10.1124/mol.116.107755
This article has not been copyedited and formatted. The final version may differ from this version.

demonstrated longer serum residence times, suggesting that a once daily dosing might be sufficient for achieving the desired therapeutic serum concentration. The pharmacokinetic data were further supported by crystallographic studies with compound II and WT RT. Similar to compound I (Frey et al., 2015), compound II makes extensive contacts with residues within the NNBP, further supporting its high potency, and suggested that compound II could be active against a range of clinically challenging variants. Hence, this study provides strong evidence that compound I and II are promising anti-HIV drug candidates and should be tested further to determine their efficacy in animal models of HIV infection.

Molecular Pharmacology Fast Forward. Published on February 6, 2017 as DOI: 10.1124/mol.116.107755
This article has not been copyedited and formatted. The final version may differ from this version.

Materials and Methods

Synthesis of Compounds I and II

The synthetic procedures for preparation of compound I and compound II have been previously described in detail (Bollini et al., 2011; Lee et al., 2014).

Animals.

Six- to eight-week-old female BALB/c mice from Jackson laboratories were used. All mice were housed in cages containing water, food and bedding. All procedures were approved by Yale University Animal Care and Use Committee.

Inhibition Assay with Pico Green and Solubility Measurements for Compounds I and II.

Inhibition assays were carried out with the PicoGreen Enzcheck Reverse Transcriptase Assay Kit (Life Technologies) as described previously (Gray et al., 2015). The compound solubility was measured using a shake-flask procedure as described previously (Bollini et al., 2013; Lee et al., 2013)

Anti-HIV activity in infected TZM-bl cells

The *in vitro* anti-HIV-1 activity of compound II was determined using a luciferase reporter gene assay (Montefiori, 2009). Twenty-four hours prior to infection, 20,000 TZM-bl cells were seeded per well in 48-well plate. Two hours before infection, the cells were incubated with medium containing compound II at concentrations ranging from 0.1pM to1μM at 37°C. The cells were infected with HIV-1 JR-CSF (MOI-0.1) 2h later and cultured for 48 hours. Luciferase activity in cell lysates were measured using the luciferase assay kit following manufacturer's protocol (Promega).

In vitro Pharmacological Profiling

In vitro pharmacological profiling of efavirenz and compounds I and II were carried out by Eurofins Groups (Cerep and Eurofins Panlabs) in a panel of enzyme and radio-ligand assays with 34 targets. The detailed information of the assays can be obtained by clicking on the direct

Molecular Pharmacology Fast Forward. Published on February 6, 2017 as DOI: 10.1124/mol.116.107755
This article has not been copyedited and formatted. The final version may differ from this version.

link provided in the Supplementary Table 1. These links will direct the readers to Eurofins Panlabs webpage where information about each assay has been provided in detail.

Crystallization, Data collection, Structure Determination and Refinement

Recombinant RT52A enzyme was expressed and purified to homogeneity using methods described previously (Das et al., 2008; Frey et al., 2012). Crystals of RT52A in complex with compound II were prepared using similar methods as the catechol diether complexes (Frey et al., 2012). The final optimized condition for crystal growth consisted of 18% (w/v) PEG 8,000, 100 mM ammonium sulfate, 15 mM magnesium sulfate, 5 mM spermine, and 50 mM MES pH 6.0. Crystals were transferred to a cryo-solution containing 27% (v/v) ethylene glycol and flash cooled with liquid nitrogen.

Diffraction data for the best crystals were collected at APS on beam line 24-ID-E through NE-CAT. High-resolution data sets for the best diffracting crystals were processed with HKL2000 (Otwinowski and Minor, 1997). In order to obtain phases, molecular replacement was performed with Phaser (McCoy et al., 2007) using a previously determined RT:NNRTI complex (PDB code: 4WE1) as the search model (Lee et al., 2014). The program Coot (Emsley et al., 2010) was used for model building into the electron density. Structure was refined using Phenix (Adams et al., 2010) until acceptable R-factors, geometry statistics (ideal RMSD for bonds and angles), and Ramachandran statistics were achieved. Iterative build, composite omit electron density maps were generated using Phenix Autobuild (Terwilliger et al., 2008). PyMOL molecular viewer (DeLano, 2009) was used to visualize, analyze the structure, and generate figures. Crystallography programs were compiled by SBGrid (Morin et al., 2013)The atomic coordinates and structure factors are deposited in the PDB with codes 5TW3

Pharmacokinetic Studies of Compound I and II in BALB/c Mice

Stock solutions of compound I and compound II were diluted in PBS containing 10% Tween 80 and administered intraperitoneally (i.p.) at a dose of 20 mg/kg and 100 mg/kg. A cohort of three

Molecular Pharmacology Fast Forward. Published on February 6, 2017 as DOI: 10.1124/mol.116.107755
This article has not been copyedited and formatted. The final version may differ from this version.

mice per group was used for pharmacokinetic measurements. A sample size of 3 animals was used based on previously published pharmacokinetic studies with NNRTIs. Additionally, lack of mortality or morbidity in our pilot experiments conducted with different doses (5 mg/kg, 10mg/kg, 20 mg/kg and 100 mg/kg) of compounds I and II suggested that n=3 would be sufficient to get statistical significant data without using higher number of animals.

Serum samples were obtained from blood collected from the ocular venous plexus by retro-orbital venipuncture at various time points after i.p. injection and used for analysis as detailed below.

Toxicity Studies of Compound II in BALB/c Mice

In acute toxicity studies, three mice were treated with single i.p bolus injection of vehicle (DMSO) or compound II at 100 mg/kg. Mice were allowed free access to food and water throughout the experiments and were monitored daily for 3 days for morbidity and mortality.

Determination of Serum Compound I and Compound II Concentrations by Quantitative HPLC

Efavirenz (5µg/mL) and nevirapine (1µg/mL) were used as internal standards for the analysis of compound I and compound II, respectively. The compounds were extracted following previously published extraction protocols with modifications (Weller et al., 2007). 200 µL of 0.01M sodium hydroxide was added to all samples and vortexed briefly followed by the addition of 1 ml of methyl-*tert*-butyl-ether (MTBE). The samples were then vortexed briefly and were placed on ice for 5 minutes to separate the MTBE layer. The MTBE layer was collected in a glass tube and dried under nitrogen at room temperature. The residue was reconstituted in 50 µL of acetonitrile and 25 µL of the reconstituted sample was subjected to analytical HPLC. The serum levels of compound I and compound II were determined using 210 Varian Prostar HPLC system (Agilent Technologies) equipped with a 218/SD-1 pumps, a PS 325 UV-Vis detector, a fraction collector (440 LC) and a computer with Open Lab CDS (Chemstation edition) software for data analysis. The C-18 analytical column (Varian Polaris 5, 150 × 4.6 mm)

Molecular Pharmacology Fast Forward. Published on February 6, 2017 as DOI: 10.1124/mol.116.107755
This article has not been copyedited and formatted. The final version may differ from this version.

was equilibrated prior to data collection with 1% A and 99% B (where A is HPLC grade water and B is HPLC grade acetonitrile). The employed linear gradient mobile phase (flow rate= 1.0 ml/min) was as follows: 95% A - 5% B at 0 min, 1% A - 99% B at 30 min, and 95% A - 5% B at 35 min. The detection wavelengths were 280 nm and 272 nm for compound I and compound II, respectively, and the response time was set at 2.0 sec. The lowest limit of detection was 25 ng/mL for compound I and 50 ng/mL for compound II. Good linearity was observed between concentrations ranging from 50 ng/mL-100 µg/mL for compound I and 25 ng/mL-100 µg/mL for compound II in serum. The calculated extraction efficiency was 65-70% for both the compounds.

Pharmacokinetic Analyses

The data were plotted as a concentration-time curve using PRISM 7.0. The predicted area under the concentration-time curve ($AUC_{predicted}$) was calculated based on the linear trapezoid method (Bourget and Delouis, 1993). The maximum concentration (C_{max}) and maximum time at which C_{max} was observed (T_{max}) were also calculated from the concentration-time curve. The total body clearance value (CL) was obtained by the following equation (Ratain and Plunkett, 2003):

Clearance value (CL) = Dose / $AUC_{0\text{-last}}$ (equation 1)

Molecular Pharmacology Fast Forward. Published on February 6, 2017 as DOI: 10.1124/mol.116.107755
This article has not been copyedited and formatted. The final version may differ from this version.

Results

HIV-1 Inhibitory Activity and Solubility Measurements for Compounds I and II

Intrinsic enzymatic inhibitory activities of compounds I and II against WT RT are compared to rilpivirine and efavirenz in Table 1. Consistent with their high potency observed in the cell-based assays (Lee et al., 2014), both compounds I and II showed single digit nanomolar IC_{50} values against WT RT. Table 1 also compares the solubility values of compounds I and II with that of rilpivirine and efavirenz. The solubility of rilpivirine was below 1 µg/mL, which is well outside the normal range of 4-4,000 µg/mL (Bollini et al., 2013; Jorgensen and Duffy, 2002). Compound I had a much higher solubility of 510 µg/mL, whereas the solubility values for compound II was slightly better than efavirenz, 82.9 µg/mL versus 68 µg/mL. The cLogP values for compound I and II were below 4 and in the normal range of 0-5 for oral drugs (Jorgensen, 2009) while efavirenz was 4.6 and rilpivirine was above 5 (Lee et al., 2014; Lee et al., 2013).

Binding Mode of Compound II in WT (RT)

To elucidate the specific interactions between compound II and residues in the non-nucleoside binding pocket (NNBP), the crystal structure of the RT: compound II complex was determined. The best crystal diffracted to amplitudes extending to a resolution of 2.85 Å, and phases were obtained via molecular replacement using the structure of RT in complex with the non-halogenated version of compound II (PDB code: 4WE1) as a search model (Lee et al., 2014). Data collection and refinement statistics are listed in Table 2. The electron density of compound II can be clearly seen in the NNBP (Figure 2). The overall conformation of compound II and the binding pocket is very similar to what we have observed previously with other RT:catechol diether complexes (Frey et al., 2012; Frey et al., 2014; Frey et al., 2015; Lee et al., 2014; Lee et al., 2013) (Figure 3). The NNBP adopts an open-cleft conformation and features three channels described as entrance, groove, and tunnel (Ekkati et al., 2012). The naphthyl moiety of compound II forms extensive van der Waals interactions with P95, L100, V108, Y188,

Molecular Pharmacology Fast Forward. Published on February 6, 2017 as DOI: 10.1124/mol.116.107755
This article has not been copyedited and formatted. The final version may differ from this version.

W229 and L234. In particular, the naphthyl ring forms an offset face-to-face π-π interaction with Y188, and a face-to-edge π-π interaction with W229. The cyano group attached to the naphthyl resides in the tunnel region protruding to the polymerase active site. The central catechol ring forms van der Waals interactions with K103 and Y181, and the backbone of K101, Y188 and G190. The ring forms an offset face-to-face π-π interaction with Y181. The F on the catechol ring protrudes into the entrance site and contacts K103 as well as V179. The uracil moiety resides in the groove region and contacts K102, K103, F227, L234, H235, P236 and Y318. The C2 carbonyl forms weak hydrogen bonds with the side chain amino group of K102 (3.5 Å N-O distance) and backbone amide of K103 (3.3 Å N-O distance).

In vitro Pharmacological Profiling

In vitro pharmacological profiling was carried out to identify off-target effects responsible for high attrition rate in drug-discovery and development process. Our compounds along with efavirenz were subjected to a panel of 34 targets, which included various receptors, ion channels, enzymes and hormones. A complete list of the targets evaluated for potential off-target effects is shown in Supplemental Table 1.

A heat map was generated based on the significant response obtained from these assays (Figure 4). The green squares represent less than 50% binding or inhibition and the red squares represent more than 50 % inhibition. In case of efavirenz, significant response of more than 50 % was noted for calcium channel L-Type, dihydropyridine (DHP channel), serotonin (5-hydroxytryptamine)(5HT2B) and sodium channel, site 2 (Na channel) assays whereas compound I showed no adverse response to all the targets tested. Similar to compound I, compound II also had no adverse response to any of the targets tested except for cytochrome P450 2C19(CYP2C19) where a little over 50 % response was seen.

Pharmacokinetics of Compound I in BALB/c mice

The serum concentration-time profile showed that the maximum concentration of compound I in BALB/c mice administered a single dose of 20 mg/kg by the i.p. route resulted in

Molecular Pharmacology Fast Forward. Published on February 6, 2017 as DOI: 10.1124/mol.116.107755
This article has not been copyedited and formatted. The final version may differ from this version.

a C_{max} of 0.54 ± 0.02 µg/mL at 4 h that persisted for up to 24 h and slowly waned in the next 24 h (Figure 5 and Table 3). An $AUC_{0\text{-last}}$ value of 13.1 ± 0.4 µg.h/mL was obtained for compound I by linear trapezoid method. The clearance level (CL) calculated using equation 1 was 25.4 min/mL/kg. Thus, a 4,000-fold higher serum concentration of compound I compared to its EC_{50} in MTT cells was rapidly achieved and maintained for more than 24 h after i.p. administration of the 20 mg/kg dose of compound I.

Pharmacokinetics and Toxicity of Compound II in BALB/c Mice

The serum concentration-time curve for compound II determined at 20 mg/kg dose showed a C_{max} of 11.8 ± 0.7 µg/mL at 4 h (Figure 6 and Table 3). An $AUC_{0\text{-last}}$ value of 201.7 ± 23.4 µg.h/mL and CL of 1.6 min/mL/kg were calculated similarly. Thus, higher levels of compound II in serum were rapidly achieved and maintained for almost 48h after i.p. administration of the 20 mg/kg dose of compound II. Additionally, we also looked at the pharmacokinetics of a single high dose of 100 mg/kg of compound II in BALB/c mice (Figure 7). A C_{max} of 52.3 ± 5.3 µg/mL at 4 h and a $AUC_{0\text{-last}}$ value of 896.4 ± 50.71 µg.h/mL were obtained. The CL of 1.8 min/mL/kg was observed which was similar to one seen with 20 mg/kg dose. These mice were also observed for 96 h for any sign of toxicity in terms of morbidity or mortality. All the treated mice remained healthy throughout the 96 h observation period, with no evidence of morbidity or clinical distress, suggesting that the single-bolus dose of compound II was nontoxic to BALB/c mice at dose levels of 100 mg/kg.

Anti-HIV activity of compound II in infected TZM-bl cells

Our previous assay for HIV infection was based on cell death induced by HIV replication in MT2 cells and cell viability measured in MTT assays as readout for antiviral potency (Lee et al., 2014; Lee et al., 2013). We also performed antiviral assays in a TZM-bl indicator cell line that expresses a luciferase reporter driven by the HIV LTR and thus a linear measure for HIV infection. TZM-bl cells were preincubated with compound II for 2 hours followed by infection with HIV-1 JR-CSF strain at an MOI of 0.1 to assess the antiviral potency of compound II. Figure 8

Molecular Pharmacology Fast Forward. Published on February 6, 2017 as DOI: 10.1124/mol.116.107755
This article has not been copyedited and formatted. The final version may differ from this version.

depicts concentration-dependent inhibition of HIV-1 infection and EC_{50} of 3.5 nM for compound II, comparable to low EC_{50} observed in the MTT assays (Lee et al., 2013). Effective inhibition of HIV JR-CSF infected cells reinforced the fact that compound II has potent inhibitory activity against HIV-1. These results encourage animal infection experiments given the favorable toxicity profile and pharmacokinetics of compound II.

Molecular Pharmacology Fast Forward. Published on February 6, 2017 as DOI: 10.1124/mol.116.107755
This article has not been copyedited and formatted. The final version may differ from this version.

Discussion

Compounds I and II were derived from a low-micromolar hit in a virtual screen by docking (Bollini et al., 2011; Lee et al., 2014). The hit, which contained a diphenylmethane substructure, was subjected to extensive analyses using free-energy perturbation (FEP) calculations for model complexes of analogs of the hit with HIV-RT. The results led us to prepare substituted catechol diethers with a cyanovinyl group as in compound I, which yielded EC_{50}s as low as 55 pM in the infected T-cell assays. Subsequently, crystal structures were obtained that confirmed the correctness of the modeled complexes. Additional FEP-guided efforts then addressed possible replacements of the cyanovinylphenyl substructure, which led to discovery of additional novel compounds including compound II (Bollini et al., 2011; Lee et al., 2014).

These compounds are highly effective NNRTIs that have strong potential for development as new anti-HIV-1 drugs with improved antiviral efficacy and drug resistance profiles (Frey et al., 2014; Frey et al., 2015; Gray et al., 2015; Lee et al., 2014; Lee et al., 2013). As noted in Table 1, these compounds are suitable drug candidates for further pre-clinical studies due to their low effective intrinsic inhibitory activities at low nanomolar concentrations, better solubility profiles and low cLogP values compared to rilpivirine (Janssen et al., 2005; Sun et al., 2012) and efavirenz (Frey et al., 2014; Lee et al., 2014; Lee et al., 2013). Our *in vitro* pharmacological profiling of these compounds against a broad range of targets, which are associated with off- target effects in humans, has shown that these compounds exhibit little to no adverse effects on these targets (Figure 4). Importantly, compounds I and II exhibited no adverse reaction to major targets like the hERG channel, blockade of which is responsible for major cardiac arrhythmias (Bowes et al., 2012). Furthermore, these compounds show no inhibition of CYP3A4, which is the major cytochrome P450 enzyme responsible for the metabolism of the majority of currently approved drugs. Even though compound II showed inhibition of CYP2C19, it was at a high concentration of 10 μM and CYP2C19 metabolizes only

Molecular Pharmacology Fast Forward. Published on February 6, 2017 as DOI: 10.1124/mol.116.107755
This article has not been copyedited and formatted. The final version may differ from this version.

10-15% of the marketed drug in contrast to CYP3A4 (Nazir et al., 2016; Wang et al., 2016). In comparison, efavirenz in our panel showed inhibition of binding of ligands to DHP and Na channels and 5HT2B receptors, explaining some of the side effects seen with efavirenz treatment. The excellent *in vitro* pharmacological qualities of these compounds led us to evaluate the safety and toxicity profile, and pharmacokinetic profiles of these compounds in a detailed in vivo pharmacokinetic analysis in BALB/c mice.

The serum concentration-time profiles after intraperitoneal administration of compounds I and II showed that both compounds were rapidly absorbed achieving maximum concentrations which were 4000- and 15,000-fold higher, respectively, than their therapeutic / effective concentrations (EC_{50}) and 17- and 5-fold lower, respectively, than the cytotoxic concentration (CC_{50}) (Lee et al., 2014; Lee et al., 2013). Interestingly, the serum concentration-time profiles of compound I and II were notable in that concentrations of 2000-4000-fold above the required therapeutic range were achieved in serum as early as 0.5 h post-injection and were maintained for more than 24 h. The observed C_{max} of compound I was comparable to C_{max} of efavirenz observed in a similar pharmacokinetic study in BALB/c conducted by Destache et al. (Destache et al., 2010). Unlike compound I, the C_{max} of compound II was 10-fold higher compared to that of efavirenz (Destache et al., 2010) (Table 3). A plateau in serum concentration was observed for both compounds after 6 h post-injection, which was sustained for a period of 24 h (Figure 5 and 6). The plateau was followed by a rapid decline to non-detectable levels by 48 h for compound I. Interestingly, a concentration of 2.9 µg/mL was detected for compound II at 48 h, which was ~3 fold higher than efavirenz level (Destache et al., 2010). Hence, the pharmacokinetic data suggest that the longer serum residence time of these compounds makes them amenable to a daily dose regimen, as plasma concentrations of the drug would be maintained in the therapeutic range under these conditions. Additionally, no morbidities and mortalities were observed in the compound-treated mice, suggesting that the C_{max} achieved were non-toxic.

Molecular Pharmacology Fast Forward. Published on February 6, 2017 as DOI: 10.1124/mol.116.107755
This article has not been copyedited and formatted. The final version may differ from this version.

Further analyses of the pharmacokinetic data showed that the area under curve ($AUC_{0\text{-}last}$) and total body clearance (CL) values for compound I were similar to those of efavirenz (Table 3). However, for compound II a much higher $AUC_{0\text{-}last}$ value of 201.7 μg.h/mL and a much lower clearance level of 1.09 mL/min/kg compared to the clearance levels of compound I (25.4 mL/min/kg) and efavirenz (16.3 mL/min/kg) were noted in our pharmacokinetic analysis. The larger $AUC_{0\text{-}last}$ values and the lower CL value could suggest that a higher volume of distribution can be achieved by compound II and also that compound II is subjected to a slower metabolism, thereby achieving sustained levels for maintaining good virus control.

The pharmacokinetic data were further supported by crystallographic studies with RT:compound II where, compound II made extensive contacts with residues within the NNBP, further explaining its high potency, and suggesting that compound II could be active against a range of NNBP mutants. Notably, the naphthyl group of compound II interacts with both P95 and W229, located at the p66/p51 dimerization interface and primer grip, respectively. Mutations with these two residues might destabilize the RT dimer or interfere with the correct placement of the primer in the active site, leading to a significant decrease in reverse transcriptase activity and therefore viral fitness. Indeed, clinical studies and in vitro mutational analysis have shown that both residues are immutable (Auwerx et al., 2005; Ceccherini-Silberstein et al., 2005; Pelemans et al., 2000), suggesting that compound II's interactions with these two residues will be able to compensate for potential lost interactions due to other NNBP mutations. Moreover, although compound II forms a hydrogen bond with the frequently mutated K103, the hydrogen bond donor is the backbone amide of K103, suggesting that the interaction is likely maintained in a number of K103 mutations. The preliminary crystal structures of compound II in complex with Y181C mutant and K103N/Y181C double mutant show that compound II binds to these two mutants in an almost identical conformation as in WT RT (compound II and NNBP residues for WT and mutants align to RMSD < 0.4). In particular, the π-π interaction between the naphthyl group and W229, van der Waals interaction with P95, and hydrogen bond between the uracil

Molecular Pharmacology Fast Forward. Published on February 6, 2017 as DOI: 10.1124/mol.116.107755
This article has not been copyedited and formatted. The final version may differ from this version.

group and K103 or N103 are maintained in the mutant structures (unpublished data). The previous report that compound II can inhibit common NNRTI-resistant mutants with a single mutation (Y181C) or double mutations (K103N and Y181C) at low nanomolar concentrations (Lee et al., 2014) supports the present hypothesis that compound II may be effective against a number of HIV strains harboring different NNBP mutations in RT.

The good pharmacological profile of compound II compared to compound I and efavirenz makes it a great candidate for efficacy trials in animal models of HIV infection. Previously, it has been established that efficacy studies of various NNRTIs at 100 mg/kg produce more than 90% inhibition of the viral capsid core p24 protein (p24 antigen) production and higher $AUC_{0\text{-last}}$ values (Rabin et al., 1996; Stoddart et al., 2007). As such, we carried out a pharmacokinetic study for compound II at 100 mg/kg in BALB/c mice (Figure 7). A 5-fold increase in the dose caused a C_{max} increase of 4.4 fold and an $AUC_{0\text{-last}}$ increase of 4.4 fold (Table 3). These features coupled with constant plasma clearance (1.8 mL/min/kg) after high i.p. dose suggests that compound II follows linear pharmacokinetic. Since compound II was well tolerated by BALB/c mice over a period of 96 h at this high concentration, the future efficacy studies could be carried out at 100 mg/kg dose without any concern for toxicity. Additionally, compound II showed low nanomolar potency against JR-CSF strains of HIV-1 virus in the single-infectivity assay.

In summary, these findings suggest that non-toxic and therapeutic concentrations of compounds I and II can rapidly be achieved and maintained for prolonged periods in the serum of BALB/c mice. Additionally, these results strongly encourage further preclinical development of these potent catechol diether compounds and encourage studies of antiviral potency in animal models for HIV infection.

Molecular Pharmacology Fast Forward. Published on February 6, 2017 as DOI: 10.1124/mol.116.107755
This article has not been copyedited and formatted. The final version may differ from this version.

Authorship Contributions

Participated in research design: Kudalkar, Anderson, Beloor, Kumar

Conducted experiments: Kudalkar, Beloor, Chan

Performed data analysis: Kudalkar, Beloor, Chan

Synthesis of compounds: Lee, Jorgensen

Wrote or contributed to the writing of the manuscript: Kudalkar, Beloor, Chan, Anderson, Jorgensen, Kumar

References

Adams PD, Afonine PV, Bunkoczi G, Chen VB, Davis IW, Echols N, Headd JJ, Hung LW, Kapral GJ, Grosse-Kunstleve RW, McCoy AJ, Moriarty NW, Oeffner R, Read RJ, Richardson DC, Richardson JS, Terwilliger TC and Zwart PH (2010) PHENIX: a comprehensive Python-based system for macromolecular structure solution. *Acta Crystallogr D Biol Crystallogr* **66**(Pt 2): 213-221.

Auwerx J, Van Nieuwenhove J, Rodriguez-Barrios F, de Castro S, Velazquez S, Ceccherini-Silberstein F, De Clercq E, Camarasa MJ, Perno CF, Gago F and Balzarini J (2005) The N137 and P140 amino acids in the p51 and the P95 amino acid in the p66 subunit of human immunodeficiency virus type 1 (HIV-1) reverse transcriptase are instrumental to maintain catalytic activity and to design new classes of anti-HIV-1 drugs. *FEBS Lett* **579**(11): 2294-2300.

Bollini M, Cisneros JA, Spasov KA, Anderson KS and Jorgensen WL (2013) Optimization of diarylazines as anti-HIV agents with dramatically enhanced solubility. *Bioorganic & medicinal chemistry letters* **23**(18): 5213-5216.

Bollini M, Domaoal RA, Thakur VV, Gallardo-Macias R, Spasov KA, Anderson KS and Jorgensen WL (2011) Computationally-guided optimization of a docking hit to yield catechol diethers as potent anti-HIV agents. *J Med Chem* **54**(24): 8582-8591.

Bourget P and Delouis JM (1993) [Review of a technic for the estimation of area under the concentration curve in pharmacokinetic analysis]. *Therapie* **48**(1): 1-5.

Bowes J, Brown AJ, Hamon J, Jarolimek W, Sridhar A, Waldron G and Whitebread S (2012) Reducing safety-related drug attrition: the use of in vitro pharmacological profiling. *Nature reviews Drug discovery* **11**(12): 909-922.

Ceccherini-Silberstein F, Gago F, Santoro M, Gori C, Svicher V, Rodriguez-Barrios F, d'Arrigo R, Ciccozzi M, Bertoli A, d'Arminio Monforte A, Balzarini J, Antinori A and Perno CF

(2005) High sequence conservation of human immunodeficiency virus type 1 reverse transcriptase under drug pressure despite the continuous appearance of mutations. *J Virol* **79**(16): 10718-10729.

Das K, Bauman JD, Clark AD, Jr., Frenkel YV, Lewi PJ, Shatkin AJ, Hughes SH and Arnold E (2008) High-resolution structures of HIV-1 reverse transcriptase/TMC278 complexes: strategic flexibility explains potency against resistance mutations. *Proceedings of the National Academy of Sciences of the United States of America* **105**(5): 1466-1471.

de Bethune MP (2010) Non-nucleoside reverse transcriptase inhibitors (NNRTIs), their discovery, development, and use in the treatment of HIV-1 infection: a review of the last 20 years (1989-2009). *Antiviral research* **85**(1): 75-90.

de Waal R, Cohen K and Maartens G (2013) Systematic review of antiretroviral-associated lipodystrophy: lipoatrophy, but not central fat gain, is an antiretroviral adverse drug reaction. *PloS one* **8**(5): e63623.

DeLano WL (2009) PyMOL molecular viewer: Updates and refinements. *Abstr Pap Am Chem S* **238**.

Delaugerre C, Rohban R, Simon A, Mouroux M, Tricot C, Agher R, Huraux JM, Katlama C and Calvez V (2001) Resistance profile and cross-resistance of HIV-1 among patients failing a non-nucleoside reverse transcriptase inhibitor-containing regimen. *Journal of medical virology* **65**(3): 445-448.

Destache CJ, Belgum T, Goede M, Shibata A and Belshan MA (2010) Antiretroviral release from poly(DL-lactide-co-glycolide) nanoparticles in mice. *The Journal of antimicrobial chemotherapy* **65**(10): 2183-2187.

Ekkati AR, Bollini M, Domaoal RA, Spasov KA, Anderson KS and Jorgensen WL (2012) Discovery of dimeric inhibitors by extension into the entrance channel of HIV-1 reverse transcriptase. *Bioorg Med Chem Lett* **22**(4): 1565-1568.

Emsley P, Lohkamp B, Scott WG and Cowtan K (2010) Features and development of Coot. *Acta Crystallogr D Biol Crystallogr* **66**(Pt 4): 486-501.

Fellner C (2016) Pharmaceutical Approval Update. *P & T : a peer-reviewed journal for formulary management* **41**(4): 220-221.

Frey KM, Bollini M, Mislak AC, Cisneros JA, Gallardo-Macias R, Jorgensen WL and Anderson KS (2012) Crystal structures of HIV-1 reverse transcriptase with picomolar inhibitors reveal key interactions for drug design. *J Am Chem Soc* **134**(48): 19501-19503.

Frey KM, Gray WT, Spasov KA, Bollini M, Gallardo-Macias R, Jorgensen WL and Anderson KS (2014) Structure-based evaluation of C5 derivatives in the catechol diether series targeting HIV-1 reverse transcriptase. *Chem Biol Drug Des* **83**(5): 541-549.

Frey KM, Puleo DE, Spasov KA, Bollini M, Jorgensen WL and Anderson KS (2015) Structure-Based Evaluation of Non-nucleoside Inhibitors with Improved Potency and Solubility That Target HIV Reverse Transcriptase Variants. *Journal of Medicinal Chemistry* **58**(6): 2737-2745.

Fulco PP and McNicholl IR (2009) Etravirine and rilpivirine: nonnucleoside reverse transcriptase inhibitors with activity against human immunodeficiency virus type 1 strains resistant to previous nonnucleoside agents. *Pharmacotherapy* **29**(3): 281-294.

Gray WT, Frey KM, Laskey SB, Mislak AC, Spasov KA, Lee W-G, Bollini M, Siliciano RF, Jorgensen WL and Anderson KS (2015) Potent Inhibitors Active against HIV Reverse Transcriptase with K101P, a Mutation Conferring Rilpivirine Resistance. *ACS Medicinal Chemistry Letters* **6**(10): 1075-1079.

Huang B, Li C, Chen W, Liu T, Yu M, Fu L, Sun Y, Liu H, De Clercq E, Pannecouque C, Balzarini J, Zhan P and Liu X (2015) Fused heterocycles bearing bridgehead nitrogen as potent HIV-1 NNRTIs. Part 3: optimization of [1,2,4]triazolo[1,5-a]pyrimidine core via structure-based and physicochemical property-driven approaches. *European journal of medicinal chemistry* **92**: 754-765.

Janssen PA, Lewi PJ, Arnold E, Daeyaert F, de Jonge M, Heeres J, Koymans L, Vinkers M, Guillemont J, Pasquier E, Kukla M, Ludovici D, Andries K, de Bethune MP, Pauwels R, Das K, Clark AD, Jr., Frenkel YV, Hughes SH, Medaer B, De Knaep F, Bohets H, De Clerck F, Lampo A, Williams P and Stoffels P (2005) In search of a novel anti-HIV drug: multidisciplinary coordination in the discovery of 4-[[4-[[4-[(1E)-2-cyanoethenyl]-2,6-dimethylphenyl]amino]-2- pyrimidinyl]amino]benzonitrile (R278474, rilpivirine). *J Med Chem* **48**(6): 1901-1909.

Jorgensen WL (2009) Efficient drug lead discovery and optimization. *Accounts of chemical research* **42**(6): 724-733.

Jorgensen WL and Duffy EM (2002) Prediction of drug solubility from structure. *Advanced drug delivery reviews* **54**(3): 355-366.

King RW, Klabe RM, Reid CD and Erickson-Viitanen SK (2002) Potency of Nonnucleoside Reverse Transcriptase Inhibitors (NNRTIs) Used in Combination with Other Human Immunodeficiency Virus NNRTIs, NRTIs, or Protease Inhibitors. *Antimicrobial Agents and Chemotherapy* **46**(6): 1640-1646.

Lee WG, Frey KM, Gallardo-Macias R, Spasov KA, Bollini M, Anderson KS and Jorgensen WL (2014) Picomolar Inhibitors of HIV-1 Reverse Transcriptase: Design and Crystallography of Naphthyl Phenyl Ethers. *ACS Med Chem Lett* **5**(11): 1259-1262.

Lee WG, Gallardo-Macias R, Frey KM, Spasov KA, Bollini M, Anderson KS and Jorgensen WL (2013) Picomolar Inhibitors of HIV Reverse Transcriptase Featuring Bicyclic Replacement of a Cyanovinylphenyl Group. *Journal of the American Chemical Society* **135**(44): 16705-16713.

McCoy AJ, Grosse-Kunstleve RW, Adams PD, Winn MD, Storoni LC and Read RJ (2007) Phaser crystallographic software. *J Appl Crystallogr* **40**(Pt 4): 658-674.

Montefiori DC (2009) Measuring HIV neutralization in a luciferase reporter gene assay. *Methods in molecular biology (Clifton, NJ)* **485**: 395-405.

Morin A, Eisenbraun B, Key J, Sanschagrin PC, Timony MA, Ottaviano M and Sliz P (2013) Collaboration gets the most out of software. *eLife* **2**: e01456.

Nazir S, Iqbal Z, Ahmad L and Ahmad S (2016) Variation in pharmacokinetics of omeprazole and its metabolites by gender and CYP2C19 genotype in Pakistani male and female subjects. *Pakistan journal of pharmaceutical sciences* **29**(3): 887-894.

Otwinowski Z and Minor W (1997) Processing of X-ray diffraction data collected in oscillation mode. *Method Enzymol* **276**: 307-326.

Pelemans H, Esnouf R, De Clercq E and Balzarini J (2000) Mutational analysis of trp-229 of human immunodeficiency virus type 1 reverse transcriptase (RT) identifies this amino acid residue as a prime target for the rational design of new non-nucleoside RT inhibitors. *Mol Pharmacol* **57**(5): 954-960.

Permpalung N, Putcharoen O, Avihingsanon A and Ruxrungtham K (2012) Treatment of HIV infection with once-daily regimens. *Expert Opin Pharmacother* **13**(16): 2301-2317.

Rabin L, Hincenbergs M, Moreno MB, Warren S, Linquist V, Datema R, Charpiot B, Seifert J, Kaneshima H and McCune JM (1996) Use of standardized SCID-hu Thy/Liv mouse model for preclinical efficacy testing of anti-human immunodeficiency virus type 1 compounds. *Antimicrob Agents Chemother* **40**(3): 755-762.

Ratain MJ and Plunkett WK (2003) Principles of Pharmacokinetics, in *Holland-Frei Cancer Medicine* (Kufe DW PR, Weichselbaum RR, et al. ed), Hamilton (ON).

Rathbun RC and Liedtke MD (2011) Antiretroviral Drug Interactions: Overview of Interactions Involving New and Investigational Agents and the Role of Therapeutic Drug Monitoring for Management. *Pharmaceutics* **3**(4): 745-781.

Riddler SA, Haubrich R, DiRienzo AG, Peeples L, Powderly WG, Klingman KL, Garren KW, George T, Rooney JF, Brizz B, Lalloo UG, Murphy RL, Swindells S, Havlir D and Mellors JW (2008) Class-sparing regimens for initial treatment of HIV-1 infection. *The New England journal of medicine* **358**(20): 2095-2106.

Spence RA, Anderson KS and Johnson KA (1996) HIV-1 reverse transcriptase resistance to nonnucleoside inhibitors. *Biochemistry* **35**(3): 1054-1063.

Spence RA, Kati WM, Anderson KS and Johnson KA (1995) Mechanism of inhibition of HIV-1 reverse transcriptase by nonnucleoside inhibitors. *Science (New York, NY)* **267**(5200): 988-993.

Stoddart CA, Bales CA, Bare JC, Chkhenkeli G, Galkina SA, Kinkade AN, Moreno ME, Rivera JM, Ronquillo RE, Sloan B and Black PL (2007) Validation of the SCID-hu Thy/Liv mouse model with four classes of licensed antiretrovirals. *PloS one* **2**(7): e655.

Sun LQ, Qin B, Huang L, Qian K, Chen CH, Lee KH and Xie L (2012) Optimization of 2,4-diarylanilines as non-nucleoside HIV-1 reverse transcriptase inhibitors. *Bioorganic & medicinal chemistry letters* **22**(7): 2376-2379.

Terwilliger TC, Grosse-Kunstleve RW, Afonine PV, Moriarty NW, Adams PD, Read RJ, Zwart PH and Hung LW (2008) Iterative-build OMIT maps: map improvement by iterative model building and refinement without model bias. *Acta Crystallogr D Biol Crystallogr* **64**(Pt 5): 515-524.

Wang Y, Zhao X, Lin J, Li H, Johnston SC, Lin Y, Pan Y, Liu L, Wang D, Wang C, Meng X, Xu J and Wang Y (2016) Association Between CYP2C19 Loss-of-Function Allele Status and Efficacy of Clopidogrel for Risk Reduction Among Patients With Minor Stroke or Transient Ischemic Attack. *Jama* **316**(1): 70-78.

Weller DR, Brundage RC, Balfour HH, Jr. and Vezina HE (2007) An isocratic liquid chromatography method for determining HIV non-nucleoside reverse transcriptase inhibitor and protease inhibitor concentrations in human plasma. *Journal of chromatography B, Analytical technologies in the biomedical and life sciences* **848**(2): 369-373.

Footnotes

Gratitude is expressed to the National Institutes of Health [Grants AI44616, GM49551, AI112443 and AI122384] and Ruth L. Kirschstein National Research Service award Individual Postdoctoral Fellowship [AI122864]. This work is based upon research conducted at the Northeastern Collaborative Access Team beamlines, which are funded by the National Institute of General Medical Sciences from the National Institutes of Health [P41 GM103403]. Crystals screening was conducted with supports in the Yale Macromolecular X-ray Core Facility [1S10OD018007-01]. This research used resources of the Advanced Photon Source, a U.S. Department of Energy (DOE) Office of Science User Facility operated for the DOE Office of Science by Argonne National Laboratory under Contract No. DE-AC02-06CH11357.

Kudalkar and Beloor contributed equally to this manuscript.

Molecular Pharmacology Fast Forward. Published on February 6, 2017 as DOI: 10.1124/mol.116.107755
This article has not been copyedited and formatted. The final version may differ from this version.

Legends for Figures

Figure 1: Chemical structures of (A) efavirenz, (B) rilpivirine, (C) compound I and (D) compound II

Figure 2: **Omit, σ_A-weighted $2mF_o$-F_c electron density contoured to 1.0 σ for RT:compound II.** Compound II was omitted from the model to generate iterative-build omit map using the original structure factors.

Figure 3: **Stereo view of the crystal structure for compound II complexed with HIV-RT.** Residues that interact with the inhibitor are shown as green sticks. Compound II is represented by yellow sticks. Black dotted lines indicate hydrogen bonds.

Figure 4: In-vitro **pharmacological profiling of efavirenz, compound I and compound II against targets for adverse drug reactions (ADRs) as described in materials and methods**. Rows represent compounds tested and columns represent targets. Percentage inhibition at 10 μM concentration of the compounds is color-coded: <50 % inhibition of target is labeled in green and >50 % inhibition is labeled in red. Abbreviations: CYP, cytochrome P450, ADOR, Adenosine receptor, ADR, adrenergic receptor, DHP, dihydropyridine or calcium channel L-type, CNR1, cannabinoid receptor, DRD, Dopamine receptor, NMDAR, Glutamate receptor, HRH1, Histamine receptor, Imidazole I2, Imidazole I2 receptor, CHRM, Muscarinic, nACHR, nicotinic acetylcholine, OPRM, opiate μ, Phorbol ester receptor, KATP, potassium channel, hERG, the human Ether-à-go-go-Related Gene, , EP4, prostanoid receptor, Rolipram, phosphodiesterase-4 inhibitor, 5HT2B, serotonin receptor 2B, Sigma σ1 receptor, Na channel, sodium channel, NET, norepinephrine transporter

Figure 5: **Pharmacokinetics of compound I in BALB/c mice.** Serum levels of compound I were monitored after an i.p. administration of 20 mg/kg compound I in three BALB/c mice. Blood samples were collected at 0.5,1,2,4,6,12,24 and 48h and analyzed as described in the Methods section. Data points represent mean ± SD.

Molecular Pharmacology Fast Forward. Published on February 6, 2017 as DOI: 10.1124/mol.116.107755
This article has not been copyedited and formatted. The final version may differ from this version.

Figure 6: **Pharmacokinetics of compound II in BALB/c mice.** Serum level of compound II was monitored after an i.p. administration of 20 mg/kg compound I in three BALB/c mice. The blood samples were collected at 0.5,1,2,4,6,12,24 and 48h and analyzed as described in the Methods section. Data points represent mean ± SD.

Figure 7: **Pharmacokinetics of compound II in BALB/c mice administered at 100 mg/kg dose.** Serum level of compound I was monitored after an i.p. administration of 100 mg/kg compound I in three BALB/c mice. The blood samples were collected at 0.5,1,2,4,6,12,24 and 48h and analyzed as described in the Methods section. Data points represent mean ± SD.

Figure 8: **HIV-1 inhibition by compound II in TZM-bl cells**. TZM-bl cells presented with compound II at varying concentrations were infected with HIV-1 (JRCSF strain). Virus infection was measured 2 days later by measuring luciferase activity in the cells. The percentage of the luciferase activity was normalized relative to the HIV-1 infected control TZM-bl cells that were not exposed to compound II. The values are mean ± SD from three different experiments involving triplicate measurements.

Molecular Pharmacology Fast Forward. Published on February 6, 2017 as DOI: 10.1124/mol.116.107755
This article has not been copyedited and formatted. The final version may differ from this version.

Tables

Table 1. HIV-RT inhibitory activity (IC_{50} in nM), experimental aqueous solubility at pH 6.5 (S in µg/mL) and computed cLogP. Data are the mean ± S.D. from three different experiments involving triplicate measurements.

Compounds	WT (nM)	cLogP	S (µg/mL)
I	4.2 ± 0.7	3.38	510[a]
II	2.0 ± 0.4	3.84	82.9
Rilpivirine	1.5 ± 0.4	5.75	0.02[b],0.24[c]
Efavirenz	41 ± 2 [c]	4.67[a]	68 [a]

[a](Lee et al., 2014) , [b](Janssen et al., 2005) pH 7, [c](Sun et al., 2012), pH 7.4, [c](King et al., 2002)

Molecular Pharmacology Fast Forward. Published on February 6, 2017 as DOI: 10.1124/mol.116.107755
This article has not been copyedited and formatted. The final version may differ from this version.

Table 2. Data Collection and Refinement Statistics for RT (WT) in Complex with Compound II

	RT: compound II
PDB Code	5TW3
Resolution Limit (Å)	**2.85**
X-Ray Source	APS 24ID-E
Wavelength, Å	0.97915
Space group	C2
No. molecules in asymmetric unit	1
Unit cell, a,b,c in Å (α,β,γ, in °)	a=224.4, b=69.5, c=104.5, α=90, β=106.0, γ=90
Resolution range, Å	50.0-2.85
Last Shell, Å	2.90-2.85
R-sym (last shell)	0.069 (0.510)
Completeness, % (last shell, %)	99.4 (99.0)
No. of Reflections (Unique Reflections)	137490 (36173)
Redundancy (last shell)	3.8 (3.8)
Avg. I/σ (last shell)	24.2 (3.3)
Total Number of Atoms (Protein/Inhibitor/Solvent/Ions)	7757, 32, 17, 1
R-free, R-factor	0.2725, 0.2270
RMS deviation bond lengths (Å), angles (°)	0.003, 0.631
Avg. B-factor: Protein/Inhibitor/Solvent, Ions	69.4, 53.9, 54.1, 87.3
Ramachandran Favored, Allowed, Outliers (%) (MolProbity)	96.62, 3.38, 0

Molecular Pharmacology Fast Forward. Published on February 6, 2017 as DOI: 10.1124/mol.116.107755
This article has not been copyedited and formatted. The final version may differ from this version.

Table 3. Pharmacokinetic parameters of compound I and compound II in comparison to efavirenz in BALB/c mice. Data are the mean ± SD of triplicate; n, number of mice

Pharmacokinetic Parameters	**Compound I (n=3)**	**Compound II (n=3)**	**Compound II (n=3)**	**Efavirenz[a] (n=3)**
Dose (mg/kg)	20	20	100	20
C_{max} (µg/mL)	0.54 ± 0.02	11.8 ± 0.7	52.3 ± 5.7	1.8 ± 0.6
T_{max} (h)	4	4	4	4
$AUC_{0\text{-}last}$ (µg h / mL)	13.1 ± 0.4	201.7 ± 23.4	896.4 ± 50.71	20.4 ± 21.1
CL (mL/min/kg)	25.4	1.6	1.8	16.3

[a](Destache et al., 2010)

Molecular Pharmacology Fast Forward. Published on February 6, 2017 as DOI: 10.1124/mol.116.107755
This article has not been copyedited and formatted. The final version may differ from this version.

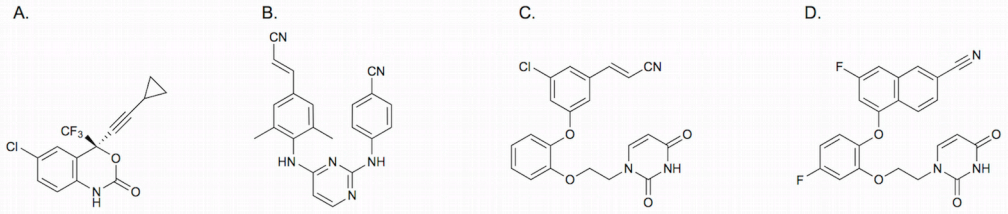

Figure 1.

Molecular Pharmacology Fast Forward. Published on February 6, 2017 as DOI: 10.1124/mol.116.107755
This article has not been copyedited and formatted. The final version may differ from this version.

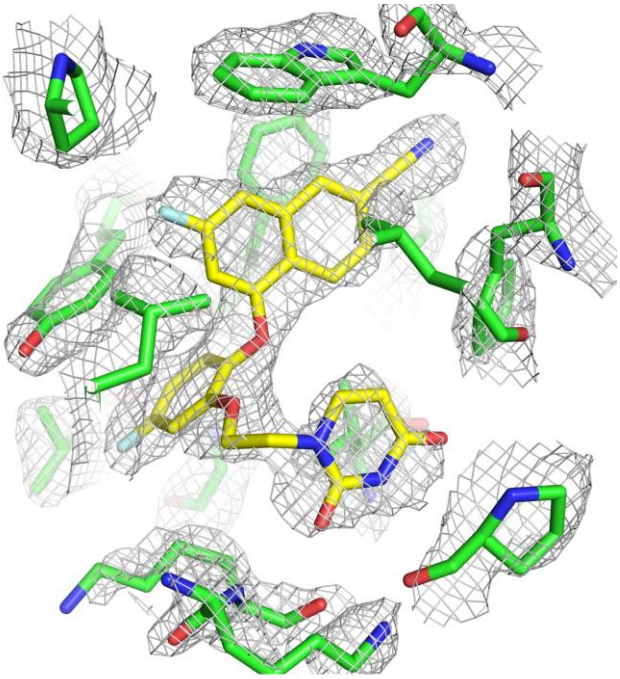

Figure 2.

Molecular Pharmacology Fast Forward. Published on February 6, 2017 as DOI: 10.1124/mol.116.107755
This article has not been copyedited and formatted. The final version may differ from this version.

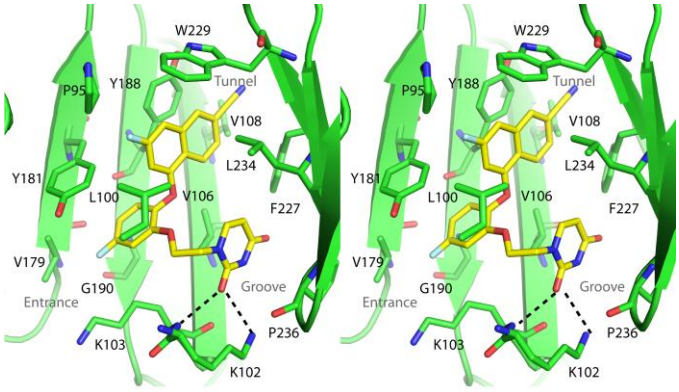

Figure 3.

Molecular Pharmacology Fast Forward. Published on February 6, 2017 as DOI: 10.1124/mol.116.107755
This article has not been copyedited and formatted. The final version may differ from this version.

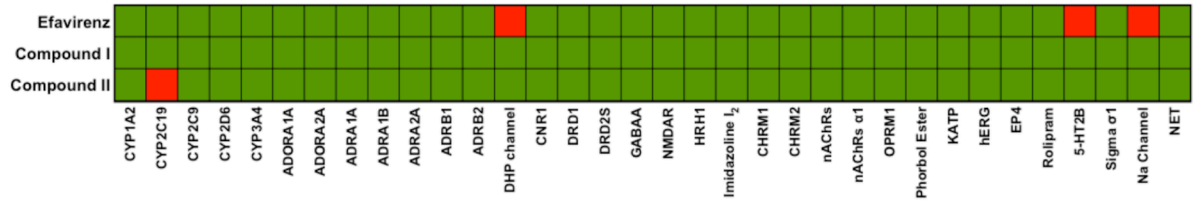

Figure 4.

Molecular Pharmacology Fast Forward. Published on February 6, 2017 as DOI: 10.1124/mol.116.107755
This article has not been copyedited and formatted. The final version may differ from this version.

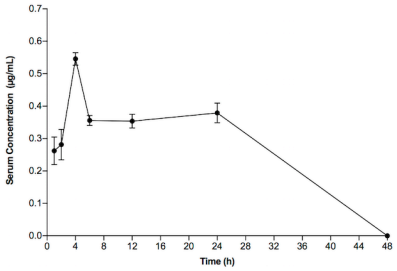

Figure 5.

Molecular Pharmacology Fast Forward. Published on February 6, 2017 as DOI: 10.1124/mol.116.107755
This article has not been copyedited and formatted. The final version may differ from this version.

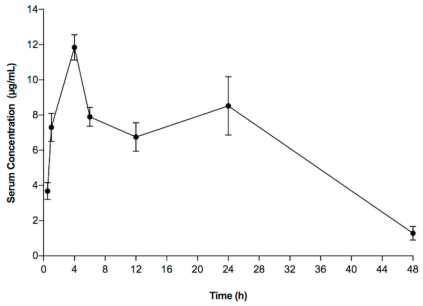

Figure 6.

Molecular Pharmacology Fast Forward. Published on February 6, 2017 as DOI: 10.1124/mol.116.107755
This article has not been copyedited and formatted. The final version may differ from this version.

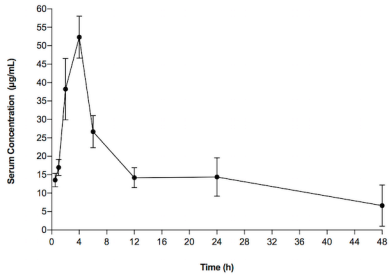

Figure 7.

Molecular Pharmacology Fast Forward. Published on February 6, 2017 as DOI: 10.1124/mol.116.107755
This article has not been copyedited and formatted. The final version may differ from this version.

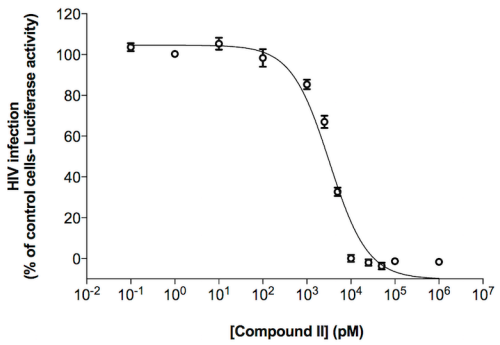

Figure 8.